Residual Stress Determination of Cast Aluminium Benchmark Components Using Strain Relief Techniques

DOI:
10.1007/s11340-024-01033-5

Document Version
Accepted author manuscript

Residual stress determination of cast aluminium benchmark components using strain relief techniques

Z. Cai[a,b], P. Mayr[c], R. Fernandez[c], S. Robbe[d], E. Usmial[d], F. Lefebvre[d], L. To[e], G. S. Schajer[e], P. J. Withers[f,b], M. J. Roy[a,b]

[a] Department of Mechanical, Aerospace and Civil Engineering, The University of Manchester, M13 9PL, Manchester, UK, [b] Henry Royce Institute, The University of Manchester, M13 9PL, Manchester, UK, [c] Nemak Linz GmbH, 4030, Linz, Austria, [d] CETIM, BP80067 60304 SENLIS Cedex, France, [e]Department of Mechanical Engineering, University of British Columbia, Vancouver, Canada, [f] Department of Materials, The University of Manchester, M13 9PL, Manchester, UK

Correspondence: Zhe Cai, Email: zhe.cai@ postgrad.manchester.ac.uk; caizhe0421@gmail.com, Tel: +44(0)161 306 6000, Fax: +44 (0)161306 3858

Abstract

Background: Residual stress development in precipitation strengthened aluminium foundry alloys has seen little attention, despite the prevalence of their use over a wide array of applications. **Objective:** This study aims at the evaluation of the residual stress in a cast aluminium benchmark that develops during precipitation heat treatment and determines the preferable stress relaxing techniques for such applications. **Methods:** The stress states in the as-cast, T4 and T6 tempers of the same AlSi7Cu0.5Mg (A356 with 0.5 wt% Cu) sample were determined through a novel application of the contour method, standard hole drilling, deep hole drilling and incremental deep hole drilling. **Results:** The results of all measurement techniques lie within approximately 40 MPa for all regions available for comparison, with the greatest differences occurring between the contour method and deep hole drilling for the T6 component. It is shown that the peak tensile residual stresses are almost identical between the heat-treated components (75 MPa), but the distribution and magnitude of compressive residual stress are found to be significantly different. **Conclusions:** Among the measurement techniques evaluated, the contour method and incremental hole drilling are found to be more suitable for T6 temper, while all techniques perform equally well for T4 temper due to its relatively low strength. It is hypothesised that the difference between the as-cast and heat-treated samples is due to solution heat treatment and quenching, while the difference in T4 and T6 tempers is attributed to the response to ageing.

Keywords: residual stress; casting; aluminium alloys; contour method; hole drilling

Introduction

Residual stresses within a finished component need to be considered both for achieving dimensional accuracy and for estimating the performance and in-service life [1][2]. Residual stresses in aluminium castings first develop during initial solidification. These stresses then evolve in a complex and difficult to predict manner during subsequent tempering, which typically consists of solution heat treatment, quenching, ageing and then final machining. This tempering process delivers the final, homogeneous properties of the component, favouring either strength or ductility. In many cases, the main source of bulk residual stress in castings stems from quenching prior to ageing. Ageing can take place either under ambient conditions (natural) or at elevated temperatures (artificial). While the former typically does not significantly change the quenched-in stresses, prolonged ageing at elevated temperature can decrease the overall residual stress state [3].

Castings tend to have much larger grains and varying texture than what wrought components have. This often excludes them from diffraction-based residual stress measurement techniques because of the small number of grains within the required sampling volume causes weak diffraction patterns. This is a particular concern for X-ray diffraction due to its small penetration depth and sampling volume. Consequently, it is usually applied in conjunction with layer removal to achieve greater measurement depth [3]. Neutron diffraction has been applied previously in the assessment of stresses developed in cast aluminium engine blocks [4], however large gauge volumes were needed to overcome an inherent coarse microstructure and texture. The effect of residual stress development in aluminium castings has also been evaluated indirectly through simulation, but without direct validation of the magnitude of residual stresses developed. To validate the predictive simulations, a combination of both strain relief and neutron methods is often required, as shown by Drezet et al. [5] when considering direct-chill casting of wrought AA 6061.

Destructive methods are generally more appropriate for stress measurements in large grained materials. The Contour Method (CM) is a well-established method for measuring residual stresses within bulk materials, but to the authors' knowledge it has not yet been reported elsewhere for measuring aluminium shape castings. This residual stress determination technique comprises carefully cutting a component in two, which allows the residual stresses to relax perpendicular to the cut plane [6]. The resulting deformed surface shapes are assumed to have relaxed elastically. After measurement, these surface shapes can be forced flat numerically to recover the stresses normal to the surface present prior to the cut. This process provides a 2-D map of the normal stresses acting on

the cutting plane that were relieved by the cut. Whilst the CM has been widely applied on a variety of components having rectangular [7] or tubular [8] cross-sections, its application to more complicated geometries having irregular profiles is under-developed at present. In such cases, the cutting arrangement as well as the subsequent modelling required to infer the stresses upon returning the cut surface to flatness is somewhat more complex. However, its ability to provide a map of stresses normal to a cross section through the casting free from some of the practical challenges posed by diffraction techniques makes it attractive. Other residual stress determination techniques either provide spot measurements at specific locations (e.g. hole drilling) or along specific paths (e.g. deep hole drilling). Furthermore, there are multiple examples of combining the CM and other techniques to recover the three orthogonal stress components at specific locations [9][10].

This paper aims to evaluate the residual stress development in precipitation strengthened aluminium castings of different tempers with a CM and HD superposition technique, and in particular, to focus on the mitigation of cutting introduced artificial stress in the application of the CM to castings with complicated geometrical profiles. To this end, as part of a residual stress measurement initiative [11], a novel application of the CM has been employed on benchmark aluminium die-cast components delivered in the as-cast (AC), naturally aged (T4) and artificially aged (T6) conditions. This has been complemented by subsequent shallow hole drilling (HD) measurements on the cut plane to determine all orthogonal stress components at specific positions by superposition. The results of this approach are then compared and contrasted with supplementary measurements made by standard shallow HD, deep hole drilling(DHD) and incremental deep hole drilling (iDHD) measurements on nominally identical components.

Experimental materials and measurement procedures

Benchmark component and measurement details

A wedge-shaped sample (Fig. 1) first introduced by Stauder [12] for sand core removal trials of permanent die castings was modified and trimmed to bounding dimensions of 107×62×90 mm³ to investigate residual stresses developed during a full casting process: casting, quenching, and a two-stage precipitation heat treatment. Thermal conditions during casting for the specimen were previously ascertained by Stauder, while additional temperature measurements during heat treatment were performed as part of this study. This makes the specimen a good candidate for residual stress assessment because individual temperature histories are well known.

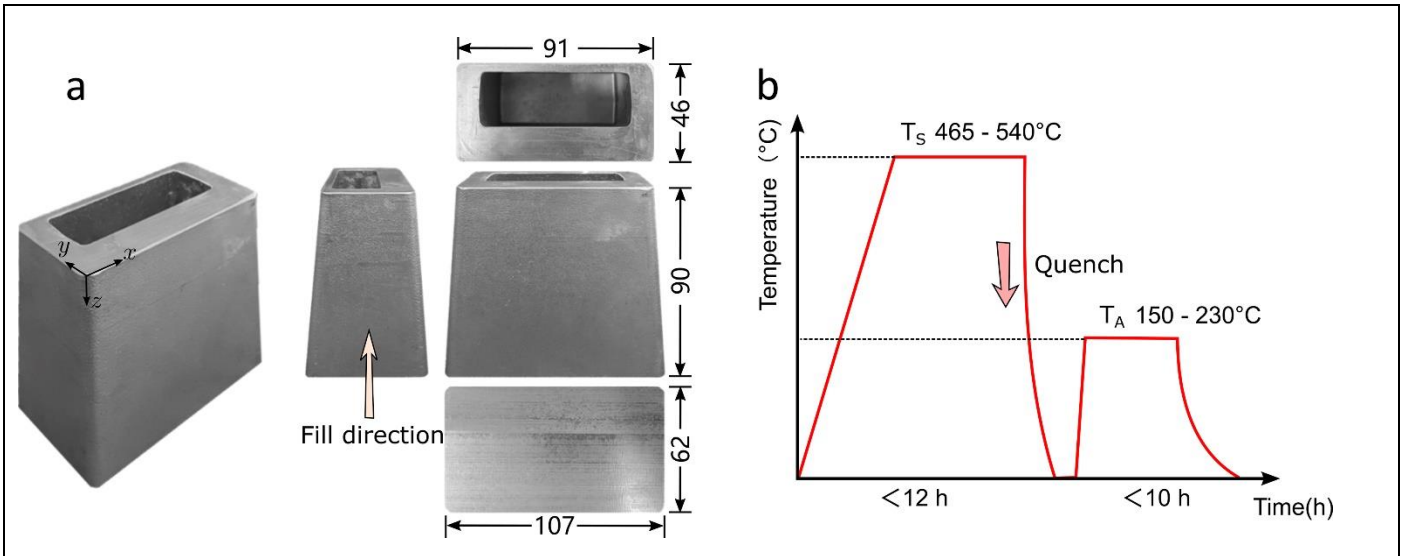

Fig. 1 a Configuration of the benchmark samples (dimensions in millimetres). A permanent steel mould with a sand core was used to produce castings under repeatable conditions. The narrow part of the wedge retained the casting surface, while the base (melt feeder location) was machined prior to heat treatment; **b** schematic showing the heat treatment cycle.

Alloy AlSi7Cu0.5Mg (A356 with 0.5 wt% Cu) corresponding to DIN EN 1706 was chosen because it is a common automotive casting alloy. First, sand cores required to shape the internal cavity of a permanent steel die were fabricated. These dies were then filled with melt that was cleaned by rotary degassing, and left to cool under ambient conditions. All samples were checked by radiography for defects before their bases were machined to final dimensions. Subsequently, the cast components were heat treated by solution heat treatment, water quenching and ageing. Minor macro-porosity was observed near the base, at the root of the internal cavity.

The local variation in mechanical properties was obtained at the thick cross-section of the component in the form of HV1 hardness measurements. The hardness of the AC as well as T4 and T6 temper castings were obtained along the middle section of the thicker-

wall side of the wedge (Fig. 2). It is clear that the hardness was significantly increased by the T4 and T6 treatments. The AC component exhibits an inhomogeneous distribution of local properties, with the base of the wedge being softer than the top. This is attributed to differences in solidification conditions and uneven cooling rate leading to the segregation of alloying ingredients and different dendritic growth conditions. After solution heat treatment and ageing, both T4 and T6 components show a much more homogeneous distribution of properties. In contrast, the naturally aged T4 component is approximately 25% softer than the artificially aged T6; the HV1 distribution in both cases is significantly more uniform than that of the AC. The yield strength of castings in each temper was measured from cylindrical samples extracted from the thick-wall side. A sample from each temper was tested to provide a 0.2% proof stresses of 120 +/- 5.6 MPa for AC, 166 +/-5.0 MPa for T4 and 277 +/-8.0 MPa for T6. Mechanical testing was carried out according to BS EN ISO 6892-1:2019, and with the range ascribed from the standard deviation of HV1 measurements as HV1 is proportional to yield strength.

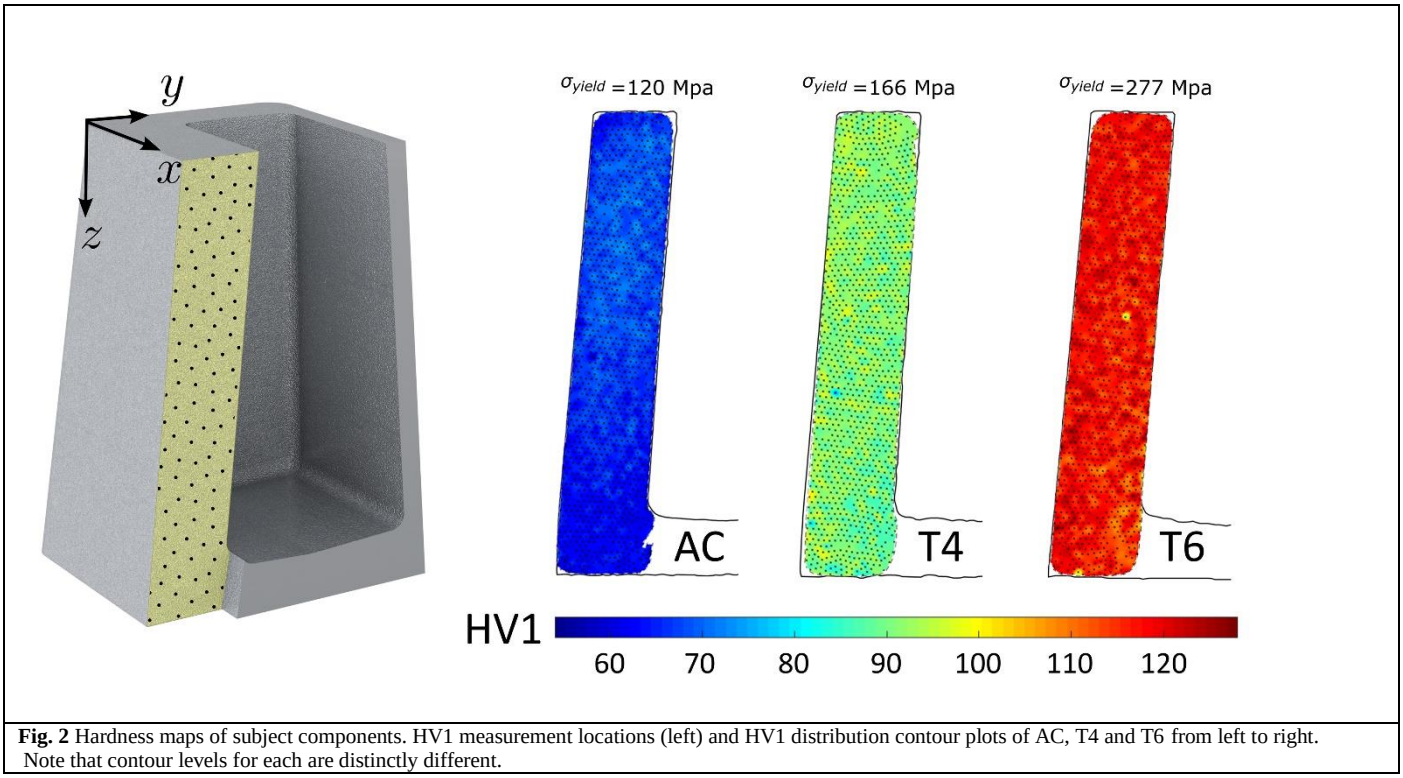

Fig. 2 Hardness maps of subject components. HV1 measurement locations (left) and HV1 distribution contour plots of AC, T4 and T6 from left to right. Note that contour levels for each are distinctly different.

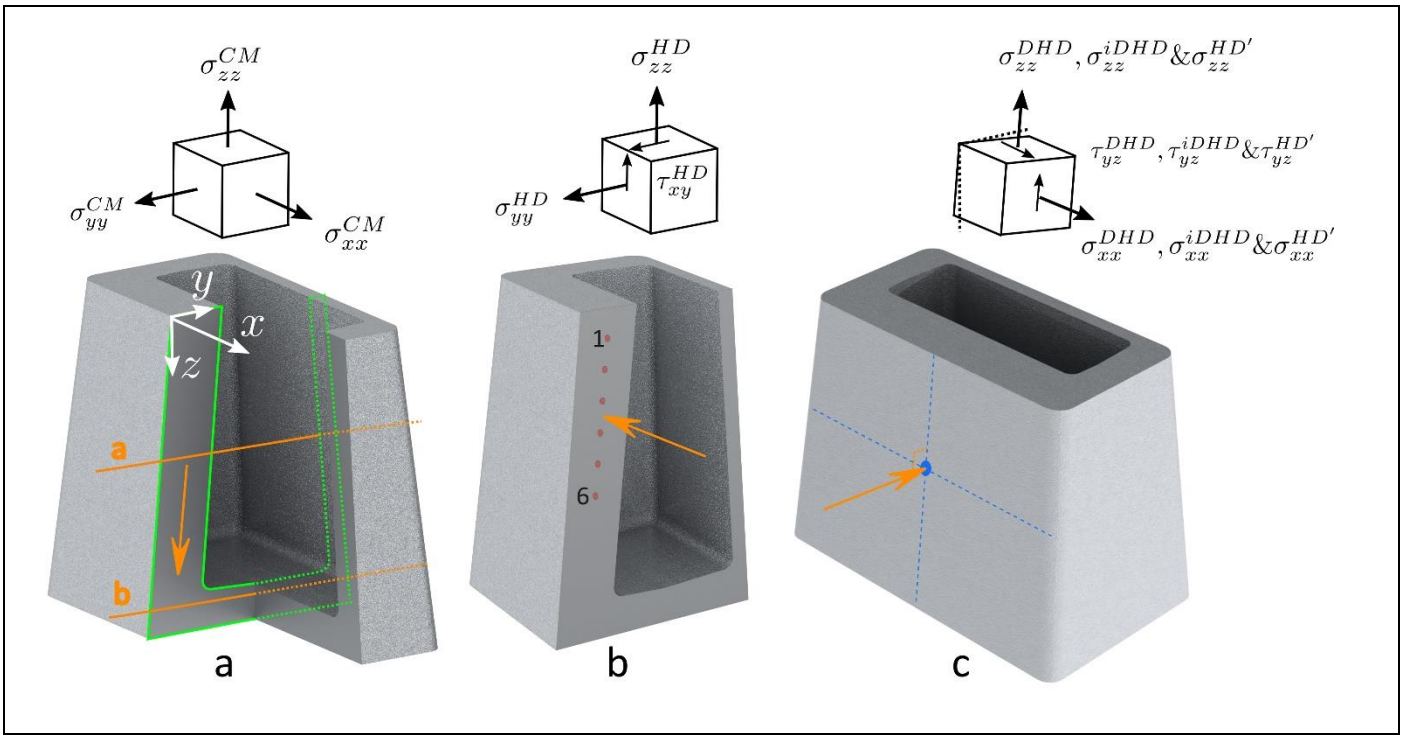

Fig. 3a CM measurement location and cutting direction. **b** HD measurement locations for the application of CM+HD superposition. **c** Standard strain gauge-based HD', DHD and iDHD measurement locations for comparison purposes.

Four types of residual stress measurements were carried out on the subject specimens. First, all specimens considered were assessed by CM (Fig. 3a), the in-plane stresses were then determined by HD at 6 positions by Electronic Speckle Pattern Interferometry (ESPI) [13]along the midpoint of the thick exposed surface of the wedge (Fig. 3b). Where applicable, CM results were compared against strain-gauge HD measurements carried out on the outer surface of the thick section for all conditions, while DHD measurements were carried out at the same location (see Fig. 3c) on the T4 and T6 components. Incremental deep hole drilling was performed on separate components at an identical location to DHD. In all cases, an elastic modulus of 74.7 GPa and Poisson's ratio of 0.33 were assumed in determining the residual stress. It is important to highlight that the region selected for measurement common to all techniques was expected to have the highest level of triaxiality in constraint during cooling, with tensile stresses expected at the centre of the thick wall such that $\sigma_{xx} > \sigma_{zz} > \sigma_{yy}$.

Contour method

Common to most CM measurements, the sample was cut by wire electrical discharging machining (WEDM), benefiting from its non-contact characteristic that minimises the stress introduced during cutting. Irregularities in cutting length will generate cutting artefacts due to the characteristics of WEDM processes [14]. Here, the cutting length is defined as the total length of instantaneous interaction between the wire and workpiece. More energy is imparted to the workpiece when the length of the cut increases on moving from a thin to thick section, for example as the cut proceeds from position *a* to *b* in Fig. 3(a). However, WEDM control architecture operates independently of the part which is being cut. Therefore, transitions between thin and thicker cutting lengths can cause localized differences in cutting width (i.e. kerf) that can be misinterpreted as stress-induced displacements, this further leads to artefacts in the resulting stresses derived by a CM analysis.

The use of sacrificial material has been advised to reduce the effect of cutting length variation in CM analysis [15][16]. This involves temporarily attaching additional material to the specimen to ensure the effective cutting thickness to be constant, and also to reduce the edge effects at wire entry and exit. Conductive epoxy is typically applied between sacrificial parts and the specimen to achieve mechanical bonding as well as to ensure there is electrical continuity along all elements in the cutting path. In the present application, due to the taper and internal draft of the subject components, the cut thickness varies significantly regardless of cutting strategy employed unless sacrificial material is used.

The cross-sectional profile along the target plane (depicted with green line in Fig. 3a) was first measured with a Mitutoyo Crysta-Apex coordinate measurement machine (CMM). Sacrificial parts were then designed to fill the inner cavity and render a rectangular outer geometry as illustrated in red on Fig. 4c. The design of the inner components was chosen so as to ensure the best fit possible, minimizing the gap requiring to be bridged by MG Chemical 8330S conductive epoxy. The interior sacrificial components were designed such that the gap between parts could be measured during layup with callipers. As the uncured conductive epoxy is thixotropic and has a published viscosity of ~5 kPa·s, the two outer components were first placed, followed by very slowly inserting the third, such that a target gap of 0.1 mm was achieved, and a uniform spew fillet was attained. Curing took place well below ageing conditions, and no measurable expansion of the gap was observed post-curing. It is assumed that the minor contraction observed during curing countered any swelling due to the published 0.3% water absorption. This approach and observations support that the component remained elastically loaded throughout the measurement and the layup did not modify the underlying stress state.

A pair of outer sacrificial parts (highlighted in blue, Fig. 4c) were applied on the outside of the component. Non-conductive epoxy was employed outside of the cutting plane as there was a good mechanical dry fit and electrical conductivity between these outer sacrificial components and the main component when clamped. Conductive epoxy was applied elsewhere to ensure that conductivity was maintained throughout the cut. A set of pilot holes were arranged on the outer sacrificial parts to minimize the relative movement of each side of the overall component during the cutting process. The assembled component prior to cutting is shown in Fig. 4a, with the cutting plane highlighted in green.

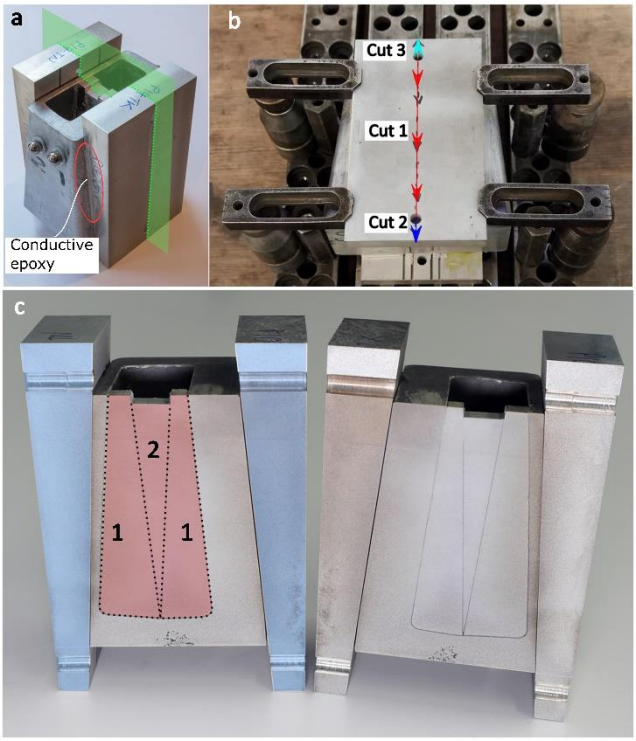

Fig. 4a Assembly of component prior to cutting (green: target cut plane; red circle: externally applied conductive epoxy), with datum features from CMM application visible. **b** Fixture arrangement and cutting sequence. **c** Resulting cut halves with sacrificial parts highlighted (red: inner sacrificial parts, with middle wedge assembled in the last; blue: outer sacrificial parts). Dashed lines indicate where conductive epoxy was applied.

Prepared specimens were cut by WEDM using a 250 µm diameter hard brass wire on an Agie-Charmilles FI440CCS CNC system. A modified 'E2' finish cut parameters for generic aluminium was used. Rigid clamping during cutting was applied at four corners of the outer sacrificial parts as shown in Fig. 4b. Three discrete, continuous cuts were performed. The first was from the top (narrowest) of the component to the base, followed by another two cuts in the external sacrificial components to separate the assembly into two halves. A representative image of the cut surfaces obtained is shown in Fig. 4c. Cut halves were treated with 100% acetone at 35°C in an ultrasonic cleaner to separate sacrificial parts from the overall component prior to measurement. The out-of-plane displacements on the cut surface due to stress relaxation were measured with a Nanofocus µScan laser profilometer with a 30×30 µm resolution across the plane of measurement and +/-0.2 µm out of plane (see Fig. 5a).

The obtained surface profile data was processed with pyCM version 2.0 [17], an open-source software for contour method data analysis. Using this software, the point clouds of the two halves of each specimen were processed in pairs to be registered, aligned and averaged, then fitted with a common analytical surface to be used in a stress calculation within a linear elastic finite element analysis. For the surface fitting step, a bivariate spline surface was employed, with a uniform knot spacing of 10 mm in the vertical and horizontal directions. These parameters were found to alleviate spurious stress concentrations near free surfaces. It was found that this 10 mm value coincided with a balance between capturing a coherent distribution of stress, versus more highly localised fitting of data at the periphery of the cross-section. An evaluation of the fitting quality showing the variance between analytical model and averaged surface displacement data is shown in Fig. 5a. The largest variance coincided with a region containing visible macro-porosity at the base of the component.

After spline fitting, a uniform finite element analysis pre-processing step was undertaken for all samples. Approximately 600 nodes were applied equally along the outline of the component, and then a 3D mesh was extruded 50 mm from the 2D profile with a geometric distribution of elements along the extrusion direction. This generated approximately 60,000 C3D8 elements for each analysis. This 50 mm dimension matches the internal void length of the component such that the mesh replicates the actual component geometry (Fig. 5b). Including the end wall of the component was not required, as it was deemed unnecessary based on the 'die-off' length [18] obtained in the final analysis for all samples. Rigid body boundary conditions were applied (Fig. 5c) in order to restrict all movements vertically on one corner of the baseplate and also in the horizontal and vertical directions on the other corner. Nodal displacements in the out of plane direction were applied from the analytical surface fitted to the averaged surface displacements.

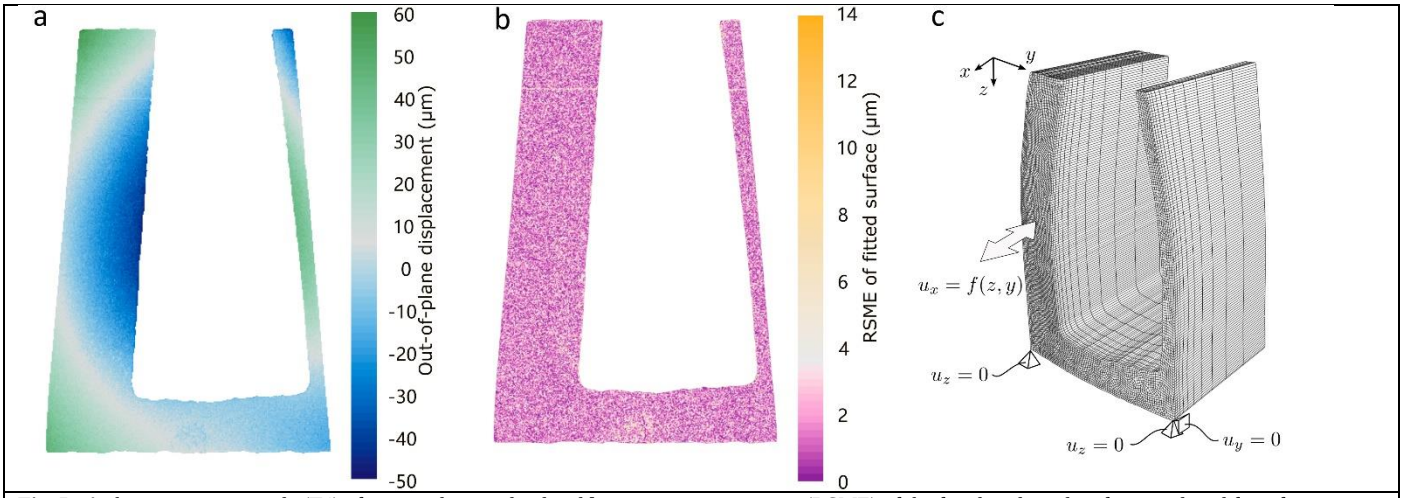

Fig. 5a A characteristic example (T4) of averaged point cloud and **b** root mean square error (RSME) of the fitted analytical surface employed for **c** finite element boundary conditions. Typical mesh employed along with boundary conditions depicted (right). Surface boundary conditions are multiplied by 100 times in the x direction, with rigid body boundary conditions in the y and z orientations.

ESPI hole drilling and stress superposition

The original in-plane stresses σ_{yy} and σ_{zz} on the contour cut surface are not fully released during the WEDM contour cutting process, so the remaining in-plane stress components (σ_{yy}^{HD}) and (σ_{zz}^{HD}) were assessed by six HD measurements made by ESPI on the cut surface (Fig. 3b). ESPI measurements were made using a PRISM residual stress interferometer (American Stress Technologies, Pittsburgh, PA). Holes of 1.82 mm diameter were drilled along the centre line of the thick side, each hole drilled in 0.1 mm increments to a total depth of 1.0 mm. ESPI measurements were made after each hole depth increment, thereby allowing the calculation of the residual stress profile within the 1.0 mm hole depth. Since the measurements were made commencing from the as-cut surface, they also incorporate the near-surface in-plane stresses imposed by the recast layer during WEDM process in addition to the remaining in-plane residual stresses. The effect of the recast layer was to introduce compressive residual stresses up to about -100 MPa within a depth up to 0.3 mm from the WEDM cut surface. At greater depths, the measured stresses were much smaller and fairly uniform. These deeper stresses are taken as being representative of the native material. By considering those measurements at 0.3 mm from the cut surface there are good arguments to suggest that they are not affected significantly by the recast layer arising from the WEDM. By summing the stresses inferred by returning the contour to flatness ($\sigma_{yy}^{CM}, \sigma_{zz}^{CM}$) and the HD ($\sigma_{yy}^{HD}, \sigma_{zz}^{HD}$) the original stress values (σ_{xx}, $\sigma_{yy}$and σ_{zz}) can be recovered, as demonstrated by Pagliaro et al. [9]:

$$\sigma_{xx} = \sigma_{xx}^{CM}$$
$$\sigma_{yy} = \sigma_{yy}^{CM} + \sigma_{yy}^{HD}$$
$$\sigma_{zz} = \sigma_{zz}^{CM} + \sigma_{zz}^{HD}$$

To do this, the hole drilling measurement locations were registered with CM data using the same surface metrology employed to capture the surface contour for CM analysis, with $\sigma_{xx,yy,zz}^{CM}$ averaged over the hole diameter in subsequent as determined by stresses resolved from integration points at nodal locations.

Supplementary HD, DHD and iDHD

Additional measurements were performed on the castings to compare with the CM, and CM+HD superposition techniques. These involved standard strain gauge HD, standard DHD, and iDHD. The location of application of standard HD is shown in Fig. 3c with a measurement depth of 1.75 mm. The outcome from these HD measurements provided bi-axial residual stresses $\sigma_{xx}^{HD\prime}$ and $\sigma_{zz}^{HD\prime}$, in which $\sigma_{xx}^{HD\prime}$can be directly compared to σ_{xx}^{CM} acquired in the previous CM measurement close to the edge. The drilling protocol is carried out according to ASTM E837 with specific calibration coefficients. These coefficients are obtained by finite element calculation using the program CASTOR [19]. These coefficients are a function only of the geometry of the strain gauge rosette, the geometry of the hole, the geometry of the part and the elastic properties of the material. The holes were drilled with a universal milling machine with tungsten carbide solid slot drills (3.5 mm diameter), over a depth of 1.75 mm. The deformations were measured using TML strain gauge rosettes (part No. FRS 3-11 F) connected to an MGC+ data acquisition unit.

The DHD residual stress measurement technique is a semi-invasive, mechanical strain relief technique (i.e., the strain of the component is measured during stress relief from the removal of a small amount of material). The procedure used for the DHD technique can be divided into five stages [20]:

1. Reference bushes are attached to the front and back surfaces of the component at the measurement location.
2. A 1.5 mm diameter reference hole is gun-drilled through the component and reference bushes.
3. The diameter of the reference hole is measured through the entire thickness of the component and reference bushes. These measurements were taken at 0.2 mm depths on 22.5° angular increments.
4. The material surrounding the reference hole (a core approximately 5 mm in diameter), was removed from the component using electro-discharge machining (EDM).
5. The diameter of the reference hole was re-measured through the entire thickness of the cylinder and reference bushes. Diameter measurements are taken at the same locations as those measured in step 3.

The diameter of the reference hole measured in step 3 is the diameter when stresses are present. During step 4, the stresses are relieved, hence the diameter of the reference hole measured in Stage 5 is the diameter when stresses are not present. The differences between the measured diameters in Stages 3 and 5 enable the original residual stresses to be calculated. The additional features such as the bushes employed are to prevent drill exit/entry artefacts.

As the technique is complicated by plasticity encountered either during stress relief or during gun-drilling, a modified technique called iDHD was employed to curb the impact on the resolved stresses. This technique involves the core being extracted in incremental machining steps using EDM, with the diameter of the reference hole measured between each increment. The diameters of the reference hole measured at each stage are then compared against each other and the original residual stresses present are calculated. The T4 and T6 casting had the stresses σ_{xx} and σ_{zz} measured with both DHD and iDHD at the same location. These measurements have been included for comparison with a line profile taken from the CM and one measurement from CM+HD superposition results at the corresponding location, as will be shown in the next section.

Results and discussion

The (σ_{xx}^{CM}) stress maps obtained by CM shown in Fig. 6 suggest that residual stresses only become appreciable once the casting has been tempered. The AC component shows that there is near-zero (<50 MPa) residual stress acting in the (x) direction that should show the highest magnitude. For the heat-treated components, a profile typical of a quenched component has been obtained, whereby the thermal expansion and difference in temperature between inner and outer regions creates a stress gradient. The distribution between the T4 and T6 tempers is distinctly different, with T4 showing a more sharply defined gradient between tension and compression. This is due to the different extent to which precipitation occurs, modifying the quench-induced stresses [21], as well as the rate at which yield stress changes with natural versus artificial aging.

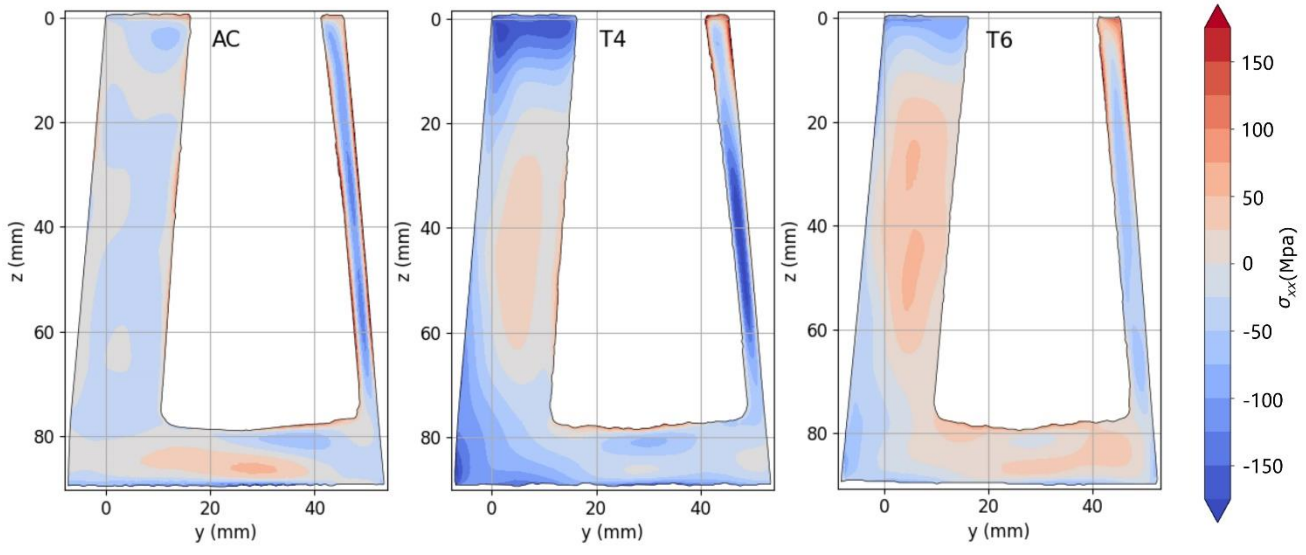

Fig. 6 Out-of-plane (σ_{xx}) stress distribution of specimen AC (left), T4 (middle) and T6 (right) determined with CM.

To substantiate the application of the CM and verify stress magnitudes obtained, Fig. 7 compares the interpolated σ_{xx}^{CM} and that found by standard strain-gauge HD, $\sigma_{xx}^{HD\prime}$, as obtained along the y direction (Fig. 3c) for all specimen types. Errors in these HD results have been reported to have a range of 90 MPa. This is very conservative, considering the relatively low stress (<50% of yield), which is significantly higher than those reported on similar applications on materials with a near-identical elastic modulus

[22]. For the purposes of a direct, legible comparison of mean results from all methods, these HD measurements have been plotted with similar error ranges as those obtained by the ESPI HD method. Good agreement is observed between the CM and HD for depths greater than 0.5 mm. Typically, CM results are deemed unreliable near-surface, usually a multiple of 2-3 times the diameter of the cutting wire i.e. 0.35 mm in this case [23] due predominantly to wire entry and exit artefacts. However, the use of sacrificial material has demonstrated that this can be minimized [16]. Departures in agreement between σ_{xx}^{CM} and $\sigma_{xx}^{HD\prime}$, particularly near the surface of the specimen are likely to be due to the fitting interval selected, mesh density employed during CM analysis and the resolution obtained of the raw surface measurements. It should be noted that there is particularly good agreement between both measurement techniques for the T4 component, with mean values overlapping, but less so for the T6. The overall T6 trend of increasing tension from the compressive surface is the same between the two measurement techniques, however the uncertainty envelopes are different. The results from hole drilling show stresses tending to be less compressive for T6 versus T4, whereas the CM results show the opposite over this near-surface region.

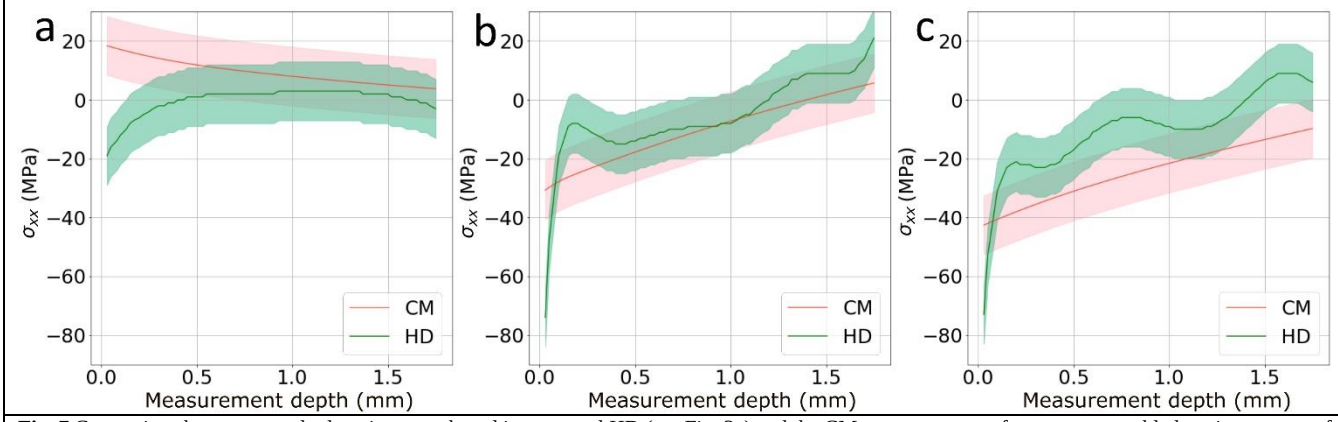

Fig. 7 Comparison between standard strain-gauge based incremental HD (see Fig. 3c) and the CM measurements of σ_{xx} at comparable locations near surface for **a** AC, **b** T4 and **c** T6. Error bars are ±10 MPa and the HD measurements extend to 1.75 mm in total.

The stresses determined by ESPI hole drilling measurements performed on the CM cut surface of three specimens are shown in Fig. 8 for location 6 (see Fig. 3b). This specific location was selected as it was expected to show the highest degree of constraint, and therefore the highest tensile stresses due to processing. For the as-cast sample, the large near surface stresses, which are in contrast to the low residual stresses in the interior, are likely due to the WEDM recast layer. At x=-0.3 mm, the stresses fall to near zero. The same trend is evident for T4 and T6, which substantiates the use of residual stress obtained at x=-0.3 mm as representative of the true residual stress. This realisation of the superposition technique differs slightly than that proposed by Pagliaro et al. [9], in that the recast layer was physically removed prior to hole drilling. Specifically, the assumption they made was that the region affected by the recast layer was 0.115 mm for a wrought aluminium component, and employing the value obtained at the 0.1 mm depth increment for superposition.

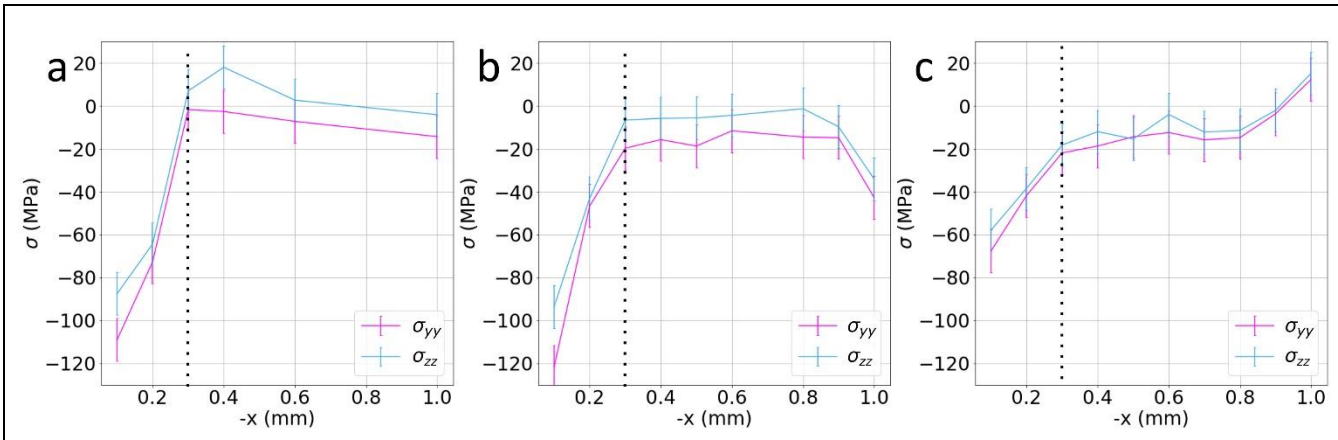

Fig. 8 Hole drilling measurements recorded at location 6 (Fig 3b) for **a** AC, **b** T4 and **c** T6. The stresses due to the WEDM recast layer are evident at depths less than 0.3 mm.

A comparison of the residual stress distribution for the AC, T4 and T6 conditions is shown in Fig. 9 for all three stress components at hole locations 1 through 6. Errors in CM results have been reported to span a total of 20 MPa as documented in interlaboratory round robin exercises performed on similar material systems and stress magnitudes [24]. Due to the two different techniques involved in the stress superposition, the error in σ_{yy} and σ_{zz} will be a sum of that in CM and HD. In agreement with the other results, the AC specimen shows near zero stresses for all components, regardless of position. This is unsurprising given that the component was left to cool slowly after casting, with little to no mechanical constraint. Therefore, at all positions and orientations, the stresses are very low, with the highest absolute mean of 20 MPa. For the heat-treated samples, the stresses for T4 and T6 are similar, particularly for orientations that demonstrate the highest stress, σ_{xx} and σ_{zz}. For these two orientations, the mean values of measurements are within 20 MPa. A noticeable difference is apparent for σ_{yy} between T4 and T6, near the top of the specimen. Overall, the assertion that $\sigma_{xx} > \sigma_{zz} > \sigma_{yy}$ is confirmed by these results as is the low stress in the AC condition.

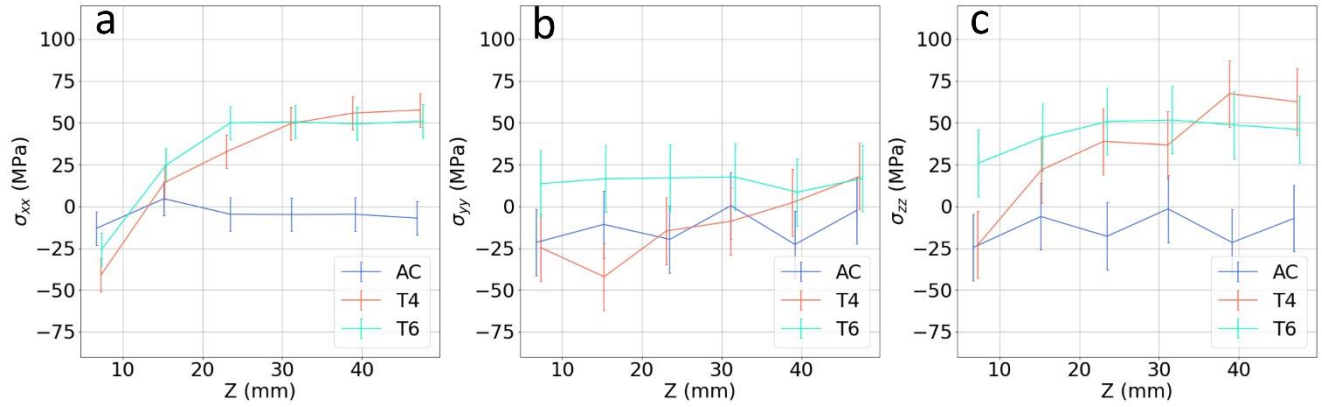

Fig. 9 Reconstructed orthogonal residual stresses **a** σ_{xx} **b** σ_{yy} and **c** σ_{zz} for each specimen at the 6 hole drilling locations employing the CM+HD superposition technique developed by Pagliaro et al. [9].

As described earlier, DHD and iDHD were applied to the two heat treated specimens at the same location as the standard (shallow) HD measurements shown in Fig. 10, providing line scans of σ_{xx} and σ_{zz} through the wall thickness of the specimen which can be compared with the CM for σ_{xx}, and the CM+HD superposition technique at a single point for σ_{zz}. For the T4 temper, excellent agreement is found for all measurements until halfway through the 16 mm cross-section. After the midway point, DHD measurements indicate more tensile σ_{xx} than those found by the CM. For the T6 condition, the difference is significantly greater: at some locations, DHD has returned tensile stresses nearly twice as much as those by CM. Further, both σ_{xx} and σ_{zz} results show a change in compression/tension gradient at the midplane. There is very little difference between results for the T4 results, particularly between the DHD and iDHD. For the T6 components, there is a significant difference between DHD and iDHD, such that the latter describes marginally lower stresses than that returned with CM and HD.

The reason for these discrepancies between the CM and HD versus DHD is believed to be due to the induced plasticity during DHD. In the first step, yielding can occur due to the drilling of the initial reference hole. In addition, plasticity can occur during the supposedly elastic relief of residual stress by trepanning, which could also introduce further stresses; e.g., the formation of a recast layer if an electro-discharge technique is employed. Although the residual stress profiles are similar between T4 and T6, the main difference is that the latter has a 25% higher yield strength. Therefore, any errors that are related to plasticity would be more pronounced in the T6 condition as opposed to T4 as higher stresses are required to cut the material. More tellingly, the main discrepancies between DHD and CM occur as the initial reference drill entered the region with the peak tensile stresses, and highest constraint and carry on beyond this point. Finally, it is difficult to see why the T6 condition should have a higher magnitude of residual stress in the DHD results (not a lower stress relative to the yield point) than T4 if it has been aged at temperatures where recovery can take place. It is shown that iDHD mitigates many of these issues seen with the T6 component, with the CM and iDHD results either matching completely, or have abutting confidence intervals.

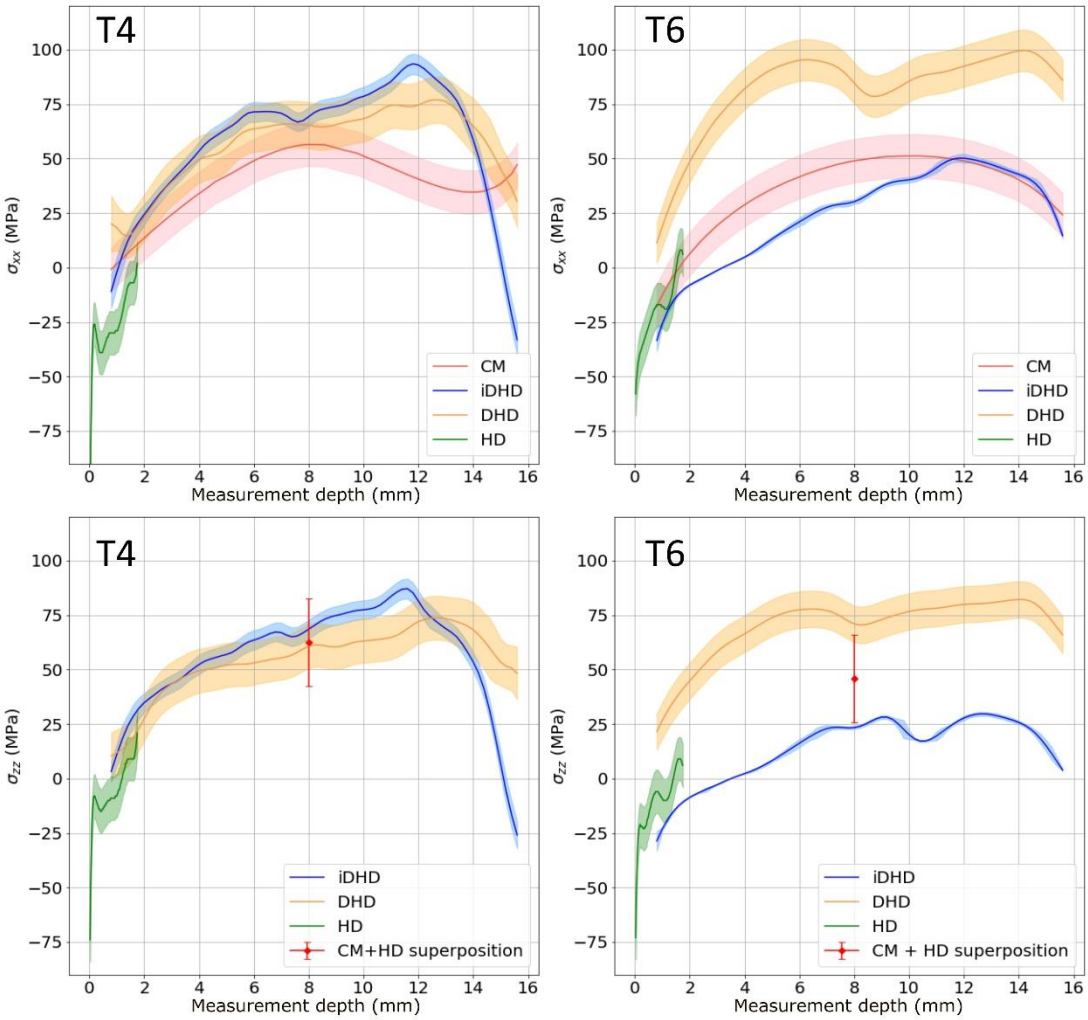

Fig. 10 Comparison of $\sigma_{xx}(y)$ and $\sigma_{zz}(y)$ between HD, DHD and CM for T4 (left) and T6 (right), plotted against the standard strain-gauge based HD measurement depth of 1.75 mm in total, and DHD measurement depth (through thickness).

Summary/conclusions

A benchmark sample for determining residual stress development in heat-treatable AlSi7Cu0.5Mg foundry alloy castings has been developed. The as cast sample was found to have very low stress levels (<50 MPa). The stresses in the heat-treated samples were much higher arising from the quenching process. Previous studies have shown that extended artificial ageing reduced the overall residual stress by recovery. The present study has found that for AlSi7Cu0.5Mg, there is little difference in the overall magnitude of stresses after ageing, but an appreciable difference in the distribution of these stresses has been found. Therefore, further consideration should be taken in the application of artificial aging as a means of residual stress mitigation as it may not effectively reduce the overall magnitude.

As it is extremely difficult to measure residual stresses in this type of material with diffraction techniques such as neutron or high energy X-rays, understanding the potential issues with applying strain relief measurements is very important to improving and predicting the service life of cast aluminium components. A good agreement was found for all measurement techniques for the low strength, high ductility naturally aged T4 temper, but less for the higher strength, lower ductility T6 temper. It is concluded that for the residual stress evaluation of such foundry alloy, the CM and iDHD remain better choices for all tempers, but extra care should be taken when the cross-sectional feature is complicated as cutting artefacts can be introduced in the cutting process of a CM analysis, this can be mitigated with proper application of sacrificial parts as demonstrated. DHD can be challenged by the elevated strength of T6 temper where plasticity is more likely to occur, but this is less of an issue for AC and T4 condition.

The three stress components are achievable with superposition technique combining the CM and HD. However, the presence of near surface stresses arising from the EDM recast layer to a depth of 0.3 mm has been identified by standard HD, and this should be considered in the selection of representative HD results.

Acknowledgements

The authors wish to acknowledge the financial support provided by the European Union's Horizon 2020 research and innovation programme under EASI Stress through grant agreement No 953219. MJR would like to acknowledge the financial support from the EPSRC (EP/L01680X/1) through the Materials for Demanding Environments Centre for Doctoral Training, and Dr. Vivek Sahu for assistance in obtaining the hardness measurements presented and VEQTER for the residual stress measurement by DHD. LT and GSS would like to acknowledge the financial support from the Natural Sciences and Engineering Research Council of Canada (NSERC). MJR and PJW are grateful to the Henry Royce Institute for Advanced Materials, founded through EPSRC grants EP/R00661X/1, EP/S019367/1, EP/P025021/1 and EP/P025498/1

Declarations

Conflict of Interest Statement: The authors declare that they have no known competing financial interests or personal relationships that could have appeared to influence the work reported in this paper.

References

[1] P. J. Withers and H. K. D. H. Bhadeshia (2001) Residual stress Part 1 – Measurement techniques. *Mater. Sci. Technol.* vol. 17, no. 4. pp. 355–365, doi: 10.1179/026708301101509980.

[2] P. Li, D. M. Maijer, T. C. Lindley, and P. D. Lee (2007) A through process model of the impact of in-service loading, residual stress, and microstructure on the final fatigue life of an A356 automotive wheel. *Mater. Sci. Eng. A.* vol. 460–461. pp. 20–30, doi: 10.1016/J.MSEA.2007.01.076.

[3] S. Salem, M. Hamed, Y. Zedan, A. M. Samuel, H. W. Doty, V. Songmene, and F. H. Samuel (2022) Evolution and Methods of Residual Stresses Measurement in Al-Si-Cu-Mg Castings: Role of Heat Treatment. *Int. J. Met.* vol. 16, no. 3. pp. 1488–1506, doi: 10.1007/S40962-021-00701-9/FIGURES/17.

[4] T. Liu, J. R. Bunn, C. M. Fancher, L. Nastac, V. Arvikar, I. Levin, and L. N. Brewer (2020) Neutron Diffraction Analysis of Residual Strain in High-Pressure Die Cast A383 Engine Blocks. *J. Mater. Eng. Perform.* vol. 29, no. 8. pp. 5428–5434, doi: 10.1007/S11665-020-05019-X/FIGURES/8.

[5] J. M. Drezet, A. Evans, T. Pirling, and B. Pitié (2013) Stored elastic energy in aluminium alloy AA 6063 billets: residual stress measurements and thermomechanical modelling. *http://dx.doi.org/10.1179/1743133611Y.0000000029*. vol. 25, no. 2. pp. 110–116, doi: 10.1179/1743133611Y.0000000029.

[6] M. B. Prime and A. R. Gonzales (2000) The contour method: Simple 2-D mapping of residual stresses, in *Sixth International Conference on Residual Stresses*, Oxford, 2000, pp. 617–624. Accessed: Oct. 14, 2021. [Online]. Available: https://www.researchgate.net/publication/286991410_The_contour_method_Simple_2-D_mapping_of_residual_stresses

[7] F. Hosseinzadeh, Y. Traore, P. J. Bouchard, and O. Muránsky (2016) Mitigating cutting-induced plasticity in the contour method, part 1: Experimental. *Int. J. Solids Struct.* vol. 94–95. pp. 247–253, doi: 10.1016/j.ijsolstr.2015.12.034.

[8] D. W. Brown, T. M. Holden, B. Clausen, M. B. Prime, T. A. Sisneros, H. Swenson, and J. Vaja (2011) Critical comparison of two independent measurements of residual stress in an electron-beam welded uranium cylinder: Neutron diffraction and the contour method. *Acta Mater.* vol. 59, no. 3. pp. 864–873, doi: 10.1016/j.actamat.2010.09.022.

[9] P. Pagliaro, M. B. Prime, J. S. Robinson, B. Clausen, H. Swenson, M. Steinzig, and B. Zuccarello (2011) Measuring Inaccessible Residual Stresses Using Multiple Methods and Superposition. *Exp. Mech.* vol. 51, no. 7. pp. 1123–1134, doi: 10.1007/s11340-010-9424-5.

[10] F. Hosseinzadeh and P. J. Bouchard (2013) Mapping Multiple Components of the Residual Stress Tensor in a Large P91 Steel Pipe Girth Weld Using a Single Contour Cut. *Exp. Mech.* vol. 53, no. 2. pp. 171–181, doi: 10.1007/s11340-012-9627-z.

[11] W. Cui, M. Sánchez Poncela, R. Badyka, P. Mayr, P. J. Withers, M. J. Roy, and R. Fernández Gutiérrez (2022) EASI-STRESS standardization of industrial residual stress measurement: benchmark specimen design, Nancy, 2022. [Online]. Available: https://hal.science/hal-03997979

[12] B. J. Stauder, H. Harmuth, and P. Schumacher (2018) De-agglomeration rate of silicate bonded sand cores during core removal. *J. Mater. Process. Technol.* vol. 252, no. October 2017. pp. 652–658, doi: 10.1016/j.jmatprotec.2017.10.027.

[13] G. S. Schajer and M. Steinzig (2005) Full-field calculation of hole drilling residual stresses from electronic speckle pattern

interferometry data. *Exp. Mech. 2005 456*. vol. 45, no. 6. pp. 526–532, doi: 10.1007/BF02427906.

[14] M. B. Prime and A. L. Kastengren (2011) The Contour Method Cutting Assumption: Error Minimization and Correction, in *Experimental and Applied Mechanics, Volume 6*, T. Proulx, Ed., New York, NY: Springer New York, 2011, pp. 233–250.

[15] X. Duan, D. Sun, A. Glover, and S. Paddea (2018) Experimental study of the weld residual stress in manually and mechanically fabricated dissimilar metal weld, in *Proceedings of the ASME 2018 Pressure Vessels and Piping Conference*, Prague, 2018, pp. 1–13. doi: 10.1115/pvp2018-84136.

[16] M. B. Toparli and M. E. Fitzpatrick (2016) Development and Application of the Contour Method to Determine the Residual Stresses in Thin Laser-Peened Aluminium Alloy Plates. *Exp. Mech.* vol. 56, no. 2. pp. 323–330, doi: 10.1007/s11340-015-0100-7.

[17] M. J. Roy, N. Stoyanov, R. J. Moat, and P. J. Withers (2020) pyCM: An open-source computational framework for residual stress analysis employing the Contour Method. *SoftwareX*. vol. 11. p. 100458, doi: https://doi.org/10.1016/j.softx.2020.100458.

[18] F. Hosseinzadeh, J. Kowal, and P. J. Bouchard (2014) Towards good practice guidelines for the contour method of residual stress measurement. *J. Eng.* vol. 2014, no. 8. pp. 453–468, doi: 10.1049/joe.2014.0134.

[19] Interactive CAE Simulation Castor Workbench - Cetim - Technical Centre for Mechanical Industry. https://www.cetim.fr/en/software/castor-workbench (accessed Jul. 06, 2023).

[20] E. J. Kingston, D. Stefanescu, A. H. Mahmoudi, C. E. Truman, and D. J. Smith (2006) Novel Applications of the Deep-Hole Drilling Technique for Measuring Through-Thickness Residual Stress Distributions. *J. ASTM Int.* vol. 3, no. 4. p. JAI12568, doi: 10.1520/JAI12568.

[21] M. J. Roy and D. M. Maijer (2014) Response of A356 to warm rotary forming and subsequent T6 heat treatment. *Mater. Sci. Eng. A*. vol. 611. pp. 223–233, doi: 10.1016/j.msea.2014.05.088.

[22] R. Richter and T. Müller (2017) Measurement of Residual Stresses: Determination of Measurement Uncertainty of the Hole-Drilling Method used in Aluminium Alloys. *Exp. Tech.* vol. 41, no. 1. pp. 79–85, doi: 10.1007/s40799-016-0129-2.

[23] M. B. Prime and A. T. DeWald (2013) The Contour Method, in *Practical Residual Stress Measurement Methods*, G. S. Schajer, Ed., John Wiley & Sons Ltd, 2013, pp. 109–138. doi: 10.1002/9781118402832.

[24] C. R. D'Elia, P. Carlone, J. W. Dyer, J. B. Lévesque, J. A. de Oliveira, M. B. Prime, M. J. Roy, T. J. Spradlin, R. Stilwell, F. Tucci, A. N. Vasileiou, B. T. Watanable, and M. R. Hill (2022) Interlaboratory Reproducibility of Contour Method Data in a High Strength Aluminum Alloy. *Exp. Mech.* vol. 62, no. 8. pp. 1319–1331, doi: 10.1007/s11340-022-00849-3.